Synergistic Effect of PARP Inhibitor and BRD4 Inhibitor in Multiple Models of Ovarian Cancer

Han Yu Huang
Shanghai General Hospital
Chen Liu
Tongji Hospital of Tongji Medical College of Huazhong University of Science and Technology
Xin Li You
Tongji Hospital of Tongji Medical College of Huazhong University of Science and Technology
Xi Li
Shanghai General Hospital
Yang chao Sun
Tongji Hospital of Tongji Medical College of Huazhong University of Science and Technology
Gang Chen (gumpc@126.com)
Tongji Hospital of Tongji Medical College of Huazhong University of Science and Technology

Research Article

Keywords: AZD5153, ovarian cancer, Olaparib, PDX, synergistic activity.

Posted Date: December 28th, 2021

DOI: https://doi.org/10.21203/rs.3.rs-1147194/v1

Abstract

Background: Ovarian cancer has the highest fatality rate among patients with gynaecological tumours. Current therapies including poly-ADP ribose polymerase (PARP) inhibitors have limitations due to the frequent recurrence of ovarian cancer after treatment and resistance to therapy.

Methods: In this study, we used multiple models with different genetic backgrounds to investigate the potential synergism effect and mechanism between the bromodomain-containing protein 4 (BRD4) inhibitor AZD5153 and the PARP inhibitor Olaparib. The models were two-dimensional (2D) and 3D cell lines, patient-derived organoids (PDO) and patient-derived xenografts (PDX).

Results: Cotreatment with Olaparib and AZD5153 exhibited marked synergistic effects, and significantly attenuated cell viability, whereas it increased DNA replication fork instability, chromosomal breakage and apoptosis compared to treatment with either drug alone. Mechanistically, the tumor upregulates PTEN after Olaparib treatment to make its DNA and chromosome more stable and therefore induces Olaparib resistance. AZD5153 can downregulate PTEN to reverse Olaparib resistance and thus increase joint lethal effect with Olaparib.

Conclusion: This study reveals that AZD5153 can downregulate PTEN to reverse Olaparib resistance and thus increase joint lethal effect on DNA replication fork instability, chromosomal breakage, and apoptosis with Olaparib.

1. Introduction

Ovarian cancer is the leading cause of cancer mortality among patients with gynaecological tumours[1]. In the past few years, new approaches have been developed to treat ovarian tumours. However, since 2017 to date, the mortality rate of ovarian cancer has shown no sign of decreasing, which demonstrates the treatment challenges. The refractoriness of ovarian cancer results from the high incidence of recurrence and drug resistance [2, 3]. clinical trials have shown that the poly-ADP ribose polymerase (PARP) inhibitors could improve the progression-free survival (PFS) of ovarian cancer patients[4, 5]. However, the wide use of Olaparib as a single agent inevitably induce resistance. Therefore, it is urgent to find solutions to delay or even reverse Olaparib resistance. Recent years, some reports have found that Bromodomain and extra-terminal motif (BET) inhibition may be a potential strategy to reverse PARP inhibitors resistance[6, 7]. The effectiveness of the combined effect of PARP and BET inhibition has been verified in different cancers. [8, 9, 10], and our previous study in ovarian cancer showed that combining the PARP inhibitor BMN673 with the BET inhibitor JQ1 resulted in a potent lethal anticancer effect [11].

The PDO model is a three-dimensional (3D) model in which human cancer tissue is cultured in vitro. Because the PDO model can be used to examine drug activity in primary tumours, it could beneficial to translational medicine studies [12, 13], and have already been used to explore drug effects in ovarian cancer [14]. The PDX model is another in vivo model that is widely used in precision medicine research [15, 16, 17],

and it retains the microenvironment and heterogeneity of the primary tumour[18]. The joint application of PDO and PDX in drug screening and mechanism exploration can be used in models to provide a closer simulation of the condition of patients [19].

In this study, we choose Olaparib and AZD5153, respectively as representative agents to further investigate the synergistic effects of PARP and BET inhibitors. Olaparib has been confirmed to show less toxicity and off-target effects clinically [20, 21] and it can be used at a high dose to achieve maximal PARP-inhibiting effect [22, 23]. AZD5153 is a more specific small molecular inhibitor of the BET protein bromodomain-containing protein 4 (BRD4) [8, 24]. The experimental models we selected were patient-derived organoids (PDO) and patient-derived xenografts (PDX), which mimic the tumour environment in patients. We not only used these models to investigate the actions of these drugs, but we also explored the mechanisms underlying these actions using experiments that are usually conducted in cell lines.

2. Methods

2.1 Cell lines and cell culture

Human ovarian cancer cell lines (HOC7、OVCAR8) were obtained from MDACC characterized Cell line Core Facility. Human ovarian cell lines (A2780, ES2, SKOV3, OVCAR3, Caov3, OV90, TOV-112D, TOV-21G) were obtained from the American Type Culture Collection (ATCC). ID8 is a mouse ovarian cancer cell line derived from C57BL/6, which was a gift by Professor K. Roby (Department of Anatomy and Cell Biology, University of Kansas, U.S.A).

Cell lines were all passaged less than 30 times and were cultured under 37℃,5% CO2 incubator. 3D cell was cultured in the same condition with PDO models.

2.2 Antibodies and compounds

Olaparib(S1060)、AZD5153(S8344) were bought from Sellek. IdU (1336001) and CIdU(C6891)were from sigma. CELLTiter GLO 3D (G9682) were from PROMEGA. Components added in the PDO culture medium are all bought from BD Biosciences. GAPDH (A19056), β-TUBULIN (AC008), α-TUBULIN (A6830), RFC4 (A5485), SMC1A(A4693) antibodies were from Abclonal. PTEN (ab267787), RFC3 (ab182143), P-SMC1A (ab75768), RAD51 (ab133534), P-CHK317 (ab226929), PI3K(ab40776), BRCA1(ab238983), BRCA2(ab239375) antibodies were from Abcam. Brd4 (#83375), γH2AX (#80312, #9718), RPA32 (#52448), P-RPA32 (#83745) antibodies were from Cell Signaling Technology (CST).

2.3 Clinical Specimens

All primary ovarian cancer tissues are anonymized and obtained from Tongji Hospital, Tongji Medical College, Huazhong University of Science and Technology, Wuhan, China, in accordance with the Declaration of Helsinki. All the operations were approved by the Ethics or Institutional Review Board.

2.4 Establishment of PDX model

PDX (Patient-derived xenografts) models were obtained by subcutaneously transplanting fresh tumor tissue into nude mice. 6-8 weeks-old female BALB/C nu-mice were purchased from Beijing HFK Bioscience and raise in specific pathogen-free conditions. All manipulations were performed under the guidance of the Animal Laboratory of Tongji Hospital. Solid tumor xenografts are passaged with the same technique after established.

2.5 Establishment of PDO model

PDO (Patient-derived organoids) models were established by using patient tissues from Tongji Hospital. Fresh tumor tissue can be stored in DMEM/F12 (1% PS) under 4 ℃ within 12 hours. The tumor tissue was minced and filtered through 70um (Falcon, #352360) and 40um (Falcon, #352340) strainer, to get a suspension of multicell-spheroid, which has a diameter between 40-100um. After treated by red cell lysis buffer and washed by PBS, the multicell-spheroid was resuspended by Matrigel (Corning, #356231). The suspension was planted into 6 or 96 well plates according to the following experiments. For example, 10 μL Matrigel with 5000 organoids per well was used for short drug screening. The Matrigel needs to solidify at 37℃ for 30 minutes, then the culture medium was added to the plates.

PDO was cultured in DMEM/F12 with Glutanmax 1×, HEPES 1×, R-spondin 100 ng/ml, Noggin 100 ng/ml, EGF 50 ng/ml, FGF10 10 ng/ml, FGF2 10 ng/ml, B27 50×, Nicotinamide 10 mmol/ml, N-Acegglytene 25 mmol/ml, ProstaglandinE2 1 umol/ml, SB02190 10 umolg/ml, A8301 500 nmol/ml and Y27632 10 μmol/ml.

2.6 Generation of PARP inhibitor resistant cells

A2780、HOC7、ID8 cells were cultured with an increased concentration of Olaparib. After 3-4 months of treatment, these cells can grow rapidly in the presence of 10uM Olaparib. Cells were cultured in the absence of Olaparib for 1 month. Before use, IC50 was calculated again to confirm its drug resistance.

2.7 Alkaline single-cell agarose gel electrophoresis (Comet) assay

Alkaline comet assay was performed by following the manufacturer's instructions of Trevigin's Comet Assay Kit (#4250-050-K). Cells were suspended in Low melting agarose and mounted on comet slides as instructed. After the gel was solidified, the comet slide was incubated in lysis solution for 1 hour at 4℃ and the freshly prepared unwinding solution for 20 minutes at room temperature in a dark place. Electrophoresis was performed under 21V for 25 minutes in the freshly prepared electrophoresis solution. Slides can be stained with SYBR Green I to analyze the comet tail, which stands for DNA strand breakage. Average damage from three independent experiments was calculated.

2.8 DNA fiber assay

Cells were labeled with 25uM CldU for 30 minutes, washed by PBS for 3 times, and then labeled with 250uM IdU for 45 minutes. After labeling, cells were collected, resuspended to 5*10^5 cells/ml in ice-cold PBS. 7ul freshly prepared spreading buffer was mixed with 2ul cell suspension and pipetted onto a

microscope slide. By carefully tilt the slides at 25-60 degrees, the stream of DNA was allowed to travel slowly down the slide. Then the slides were airdried and fixed in methanol/acetic acid (3:1) for 10 minutes. Slides were then washed with ddH2O, denatured in 2N HCL for 30 minutes, and block with 5% BSA-PBS. After that, the slides were incubated with 1:150 rat anti-BrdU (Abcam, ab6326) and 1: 50 mouse anti-BrdU (BD Biosciences, #347580) antibody for 3 hours at room temperature. Then the slides were rinsed and incubated in 1:150 anti-Rat AlexaFluor 488 antibody and 1:150 anti-Mouse AlexaFluor 568 antibody for 1 hour at room temperature. The results were obtained by using Zeiss Laser Scanning Confocal Microscope 880.

2.9 Fluorescence in situ hybridization (FISH) assay

The slides were pretreated with xylene and gradient ethanol to dewaxing and hydration, boiled, digest with 200μL pepsin solution, and then put into 2xSSC at room temperature for 3 minutes. Dehydration with gradient ethanol for 2 times and dried at room temperature. Samples and probes were hybridized in an environment protected from light. Then the slides were washed and counterstained.

The probes(LBP Guangzhou,# F.01005-01)can hybrid with chromosome 10 centromere (green signal) and PTEN gene (red signal). The normal cell contained 2 red and 2 green signals. A PTEN amplificated signal mode contains more red signals.

2.10 Metaphase spread assay

Cells were exposed to colchicine (100 ng/ml) (Sellek, S2284) for 3 hours, collected and resuspension in hypotonic solution (0.075M KCl) for 30 minutes at 37°C incubator. Cells were then fixed in methanol: acetic acid (3:1) at 4℃ for 30 minutes and repeat for 3 times. Then the fixed cells were dropped on precooled slides and put into a 65℃ incubator to air-dried. After cooled down, the slides were stained in 3% Giemsa and coded for blind analysis. A total of 25 metaphases was analyzed from each sample to detect the presence of chromosomal fragments.

2.11 NCI60, CCLE and GSCALite

Gene expression profiles (Gene transcript level z score) for correlations analysis in NCI60 human tumor cell lines were obtained using the web-based tool provided by CellMiner (http://discover.nci.nih.gov/cellminer/).

Gene mutation data of cell lines was collected from Cancer Cell Line Encyclopedia (CCLE) (https://portals.broadinstitute.org/ccle/data/browseData?conversationPropagation=begin).

The correlation between gene expression and drug reaction of human tumor cell lines were obtained by using the web-based tool provided by GSCALite (http://bioinfo.life.hust.edu.cn/web/GSCALite/). The gene expression and drug reaction data were collected by GSCALite from CCLE, CTRP and GDSC.

2.12 ChIP-Seq Analysis

ChIP-seq data for human cell lines from PMID 27803105, PMID 29491412 and GSM2090919, GSM 2090922 was collected from Cistrome (http://cistrome.org/db/#/) and analyzed by UCSC genome browser (http://genome.ucsc.edu/).

2.13 Crispr screening and mass spectrum data

Crispr screening data of Olaparib acquired resistant cell lines was downloaded from PMID29973717 and the mass-spectrum data (ID 013196) was downloaded from proteome-central(http://proteomecentral.proteomexchange.org/cgi/GetDataset?ID=PXD013196). The pathway enrichment of the data was done by using web-based tool provided by DAVID (https://david.ncifcrf.gov/summary.jsp).

2.14 Q-RTPCR

Total RNA (1 μg) was reversely transcribed into cDNA with the Hiscript Q-RT SuperMix for qPCR (Vazyme Biotech). According to the manufacture instructions. Real-Time PCR Master Mixes kit (Life Technologies) was used for the thermocycling reaction in a BioRad CFX96 Real-Time system. The mRNA levels analysis was carried out in triplicate and normalized by GAPDH. Primers sequences of PTEN were as listed.

MOUSE

FORWARD TGGATTCGACTTAGACTTGACCT

REVERSE GCGGTGTCATAATGTCTCTCAG

HUMAN

FORWARD TGGATTCGACTTAGACTTGACCT

REVERSE GGTGGGTTATGGTCTTCAAAAGG

2.15 Virus transfection protocol

In a six-well culture plate, cells are cultured at 50%-70% confluency in an antibiotic-free growth medium supplemented with FBS. The mixture was gently mixed and incubated for 30min at room temperature. Use the antibiotic-free growth medium to wash the cells twice. Add 0.2ml virus to well for each transfection. Add 40 ul Transfection Reagent Complex to well, covering the entire layer and gently swirling the plate. Incubate the cells at 37℃ in a CO2 incubator for 6 hours. Add 1ml normal growth medium containing 2 times FBS and antibiotics into each well, and incubate for 18-24 hours in 37℃, 5% CO2 incubator. Use puromycin to select stably transfected cells. PTEN shRNA and PTEN overexpression virus are bought from Genechem.

2.16 Western Blot assay

Cells were lysed with RIPA buffer (Servicebio, G2002-100) containing protease and phosphatase inhibitor cocktail (Servicebio, G2002-100). The lysates were centrifuged at 12000rpm 4℃ for 20 minutes to collect supernatants. After determining the protein content, the cell lysates were separated by 10% SDS-PAGE and electro-transferred onto 0.45um PVDF membranes. The membranes were blocked with 5% BSA-TBST at room temperature and then incubated with primary antibodies at 4℃ overnight. Secondary antibody (Antgene) was incubated for 1 hour at room temperature. Bands were visualized by using WesternBright ECL Kit (Advansta, 190113-13).

2.17 Immunohistochemistry

Immunohistochemistry was performed as previously described[11]. The primary antibody included Ki67(Abcam,1:500), RAD51(Abcam,1:500), γH2AX(Abcam,1:500).

Tumor cell staining was assigned a score using a semi-quantitative grading system: 0, 0–5% tumor-cell staining; 1, 5–25% tumor-cell staining; 2, 26–50% tumor-cell staining; 3,51–75% tumor-cell staining; and 4, >75% tumor-cell staining. Staining intensity was assigned a score using a semi-quantitative four-category grading system: 0, no staining; 1, weak staining; 2, moderate staining; and 3, strong staining. Every core was assessed individually and the mean of three readings was calculated for every case. The tumor cell staining score was determined separately by two independent experts simultaneously under the same conditions. In rare cases, discordant scores were reevaluated and scored based on consensus opinion.

2.18 In vivo small animal imaging technology

C57BL/6 mice were purchased from Beijing HFK Bioscience and raise in specific pathogen-free conditions. ID8 cells are planted intraperitoneally into mice.

Mice were anesthetized intraperitoneally with 4% chloral hydrate (g / ml) at a dose of 150ul / 20g body weight. 5mg of the fluorescent substrate was injected intraperitoneally for 10 minutes. The anesthetized and injected mice were placed in the instrument. The images were collected by the small animal imaging instrument (SIEMENS Inveon), and the same low and high values of fluorescence signals were set for each group.

2.19 Statistical analysis

GraphPad Prism 8 and IBM SPSS statistic 26.0 were used for statistical analysis. $P < 0.05$ was considered to indicate a significant difference.

3. Results

3.1 Olaparib treatment can enhance the expression of PTEN which relates to Olaparib resistance

Firstly, we analyzed the difference between Olaparib resistant and sensitive ovarian tumor tissues which were classified by PDO drug screening, we could see that PTEN changed significantly. The RNA-SEQ data implied that the relative Olaparib-resistant group had a higher PTEN expression than the sensitive group (Fig. 1A). At the genetic level, the signal mode detected by FISH assay also exhibited that PTEN had been amplificated after Olaparib resistance occurred (Fig. 1B). From the NCI-60 tumor cell line data, which was analyzed by the cell miner CDB website, it was found that the sensitivity of cells to Olaparib was negatively correlated with PTEN expression (fig.S1A). The mass spectral data of PTEN also indicated that this protein was highly correlated with DNA replication and chromosomal stability (Fig. 1C). The RFC and SMC protein families, which were overlapped between these two datasets, were related to Olaparib resistance, and affected by PTEN. Furthermore, pathway enrichment showed that pathways related to Olaparib resistance were mainly correlated to DNA replication and chromosome stability. This result agrees with the analysis of clustered regularly interspaced short palindromic repeats (CRISPR) screening data of acquired Olaparib resistant cell lines in a public database (fig. S1B).

The results of the western-blotting (Fig. 1D) show that 5 μM Olaparib treatment up-regulated PTEN, together with phosphorylated checkpoint kinase 1 (p-CHK1) and p-replication protein A 32 kDa subunit (rpa32), indicating that the DNA replication function was activated by the stress induced by drugs. To maintain the structure and function of the heredity material, the corresponding proteins also increased. The increase in RFC and SMC protein family members could be regarded as a compensatory action for cells to cope with the actions of Olaparib. We further explored this phenomenon, acquired Olaparib resistant cell lines were successfully established (fig. S1C). The acquired Olaparib resistant cell line also exhibited higher expression levels of these proteins (Fig. 1E). Immediately afterwards, we used shRNA technology and overexpression viruses to up-regulate or down-regulate PTEN expression (shPTEN, shPTEN+PTEN) in ID8, and the expression levels of PTEN protein and mRNA were significantly changed (Fig. 1F and 1G). Meanwhile, we found that the sensitivity to Olaparib was enhanced after PTEN was downregulated, while after PTEN was restored in shPTEN cell lines, the sensitivity of Olaparib decreased (Fig. 1H and 1I). The results above, we found that PTEN was essential in Olaparib resistance.

3.2 AZD5153 reverse Olaparib resistance by reducing PTEN expression

We also compared the shPTEN and original parent cell lines, and the results showed that PTEN knockout increased the endogenous DNA double strands break (Fig. 2A). This phenomenon was observed using the comet assay and suggests that PTEN had a protective effect on the DNA. The examination of the chromosomes showed that Olaparib treatment induced the repair of chromosomes in the original cell line, whereas those of the shPTEN cells exhibited complex aberrations at the same concentration of Olaparib (Figs. 2B and S1F). This result indicated that PTEN knockout played an important role in the maintenance of DNA stability and chromosomal structure, which could sensitize ovarian cancer cells to Olaparib. This is similar to the effect of AZD5153[7, 25]. So, we assume that AZD5153 may affect the sensitivity of Olaparib by reducing PTEN.

Subsequently, the chip-seq data in the public database further verified the inhibitory effect of the BRD4 inhibitor on PTEN (Fig. 2C). Tumour cells attempt to compensate for the stress caused by Olaparib by increasing PTEN expression. AZD5153 specifically targets PTEN, causing dysfunction in DNA replication and chromosome stability, and thereby enhances the sensitivity of cells to PARP inhibitors. Consistently, the effect of AZD5153 on PTEN was verified using quantitative reverse transcription-polymerase chain reaction (qRT-PCR), which showed the changes in PTEN expression levels in the cell line after drug treatment (Fig. 2D). The western blotting results also showed that AZD5153 treatment inhibited PTEN expression in cells. (Fig. 2E).

The Gene Set Cancer Analysis (GSCA) database was used to analyse the protein expression and drug sensitivity data from Cancer Cell Line Encyclopedia (CCLE), Cancer Therapeutics Response Portal (CTRP), and Genomics of Drug Sensitivity in Cancer (GDSC) databases, and the results showed that the half-maximal inhibitory concentration (IC_{50}) of BRD4 inhibitors was negatively correlated with PTEN expression (Fig. 2F). Therefore, it could be inferred that Olaparib-resistant cell lines with a higher PTEN expression would be more strongly affected by AZD5153 and be more sensitive to co-treatment than those with lower PTEN levels. The reversal of Olaparib resistance by AZD5153 could reflect the results under both 2D and 3D environments (Fig. 2G).

3.3 AZD5153 and Olaparib showed a widespread synergistic cytotoxicity in multiple ovarian cancer models

In vitro ovarian cancer models, 15 cell lines and 22 PDO models were used to test the drug effects, and the result showed a marked synergistic anti-tumour effect on both models (Figs. 3A and S2A). Among the experimental models with various genetic backgrounds, 86.7% (13/15) and 90.9% (20/22) of the cell lines and PDO models, respectively were more sensitive to co-treatment with Olaparib and AZD5153 than either drug alone.

After calculating the cell viability, we used multiple methods to comprehensively examine the structure of the spheroid and observed that it was composed of obviously dead and depolymerized cells because of the cytotoxicity of the drugs (Fig. 3B). Acridine orange and propidium iodide (AOPI) staining clearly showed that the red fluorescent-labelled dead cells were gradually depolymerized from the PDO spheroid and scattered around the green fluorescent-labelled live cells (Fig. 3C). Hematoxylin and eosin (H&E) and fluorescence staining of the PDO model also showed a decrease in the spheroid diameter and increase in depolymerized cells (Fig. 3D).

Furthermore, phosphorylated H2A.X variant histone (γH2AX) staining verified that cells in the PDO spheroid were killed by the drug co-treatment (Fig. 3E). In the co-treated group, the dissociation of dead cells and decreased in diameter of the live PDO spheroids were obviously stronger than they were in the groups treated with either drug alone. Meanwhile, the combined therapeutic effect of AZD5153 and palbociclib in 2D cell lines were also synergistic lethality (Figure S2B-S2C). The synergistic effect was also examined in the A2780 cell line where we measured the response to AZD5153, Olaparib, and their

combination under 3D conditions (fig. S2D-S2E). The results indicated that AZD5153 and Olaparib showed a widespread synergistic cytotoxicity in multiple ovarian cancer models.

3.4 Co-treatment with AZD5153 and Olaparib damaged DNA by affecting its replication

To further elucidate the mechanisms of combined lethal effect on AZD5153 and Olaparib, we established two DNA fibre assays to examine the long- and short-term drug effects on DNA replication. In the long-term assay, we treated the ovarian cancer models for 2 (cell line) or 4 (PDO model) days before performing 5-chloro-2'-deoxyuridine (CldU) and 5-Iodo-2'-deoxyuridine (IdU) labelling (Fig. 4A and B). After drug treatment, measurement of labelled DNA fibres revealed a significant decrease in CldU + IdU tract length in the ovarian cancer models (Fig. 4C and D).

The tract length in the group co-treated with both drugs was significantly shorter than it was in the groups treated with either drug alone. The calculation of replication rate [26] also indicated that AZD5153 treatment slowed the fork progression rate of the DNA fibres, which was even slower in the co-treated group than it was in the groups treated with either agent alone. The ratio of IdU to CldU indicated a steady rate of DNA fork replication [27]. The IdU/CldU ratio decreased in the drug-treated groups, especially in the co-treated group, showing that the replication forks became unsteady and easier to degrade (Fig. 4E) after treatment.

In the short-time assay, the ovarian cancer cells were treated with drugs in between the CldU and IdU labelling (Fig. 4F). The condition of the IdU tracts indicated that the drugs immediately affected DNA replication. Furthermore, the results showed that the co-treated group exhibited a typical signal pattern where the green fluorescence of the IdU tracts were much denser and shorter than those of the other groups (Fig. 4G). The groups treated only with Olaparib and only with AZD5153 exhibited a denser green signal and shorter IdU tracts, respectively than those of the control group. We also identified the following three major patterns of fibre labelling, elongated, stalled, and new firing (Fig. 4H) [28, 29].

Olaparib treatment caused the development of more new firing DNA fibres [30], whereas AZD5153 produced more stalled fibres. Furthermore, in the replicating DNA fibres, AZD5153 treatment destabilized the forks and caused them to degrade in the early phase. The combined effects of both Olaparib and AZD5153 caused more DNA fibres to break, and they were damaged further.

The change in the protein levels observed using western blotting (Fig. 4I) verified the changes observed in the DNA fibre assay. Olaparib treatment up-regulated proteins related to DNA replication stress and replication fork stability, whereas they were down-regulated by AZD5153. The protein expression levels in the co-treatment group suggested that the DNA fibres were in an unstable state. The disordered DNA replication resulted in strand breaks and the comet assay confirmed that the PDO model and cell lines showed more DNA double-strand breaks after co-treatment than they did following monotherapy with either drug (Fig. 4J and 4K).

3.5 AZD5153 and Olaparib can also cause greater damage in chromosome and lead to apoptosis.

We observed increased levels of micronuclei damage following co-treatment with Olaparib and AZD5153, which suggests a more severe chromosomal breakage (Fig. 5A). We also investigated the chromosomal damage using a metaphase spread assay (Fig. 5B) and the results showed that chromosomal fragments, breakage, and aberration were higher in the co-treated group than they were in the groups treated with either agent alone. This observation indicates that more damage occurred.

Cells with micronuclei and chromosomal breakage usually undergo apoptosis and we examined the cell status using immunofluorescence staining of the γH2AX foci (Fig. 5C). The result suggested that more cells underwent apoptosis occurred after drug treatment, whereas the western blotting also showed similar changes in protein level (Fig. 5D and 5E). Flow cytometry was also used to directly examine the apoptosis rate (Fig. 5F). Collectively, these results suggest that co-treatment induced greater cytotoxicity than treatment with either drug alone.

3.6 AZD5153 plus Olaparib delay ovarian cancer growth in vivo

Co-treatment with AZD5153 and Olaparib exhibited a similar synergistic effect in vivo. Both the patient and cell-line-derived xenografts showed a lower tumour burden after co-treatment with both drugs. We used three different subcutaneous PDX BALB/C nu-mouse models and one abdominal ID8-derived xenograft C57BL/6 mouse model to analyse the combined drug effect. The tumour volumes of the subcutaneous PDX models were significantly lower after co-treatment than after treatment with either drug alone (Fig. 6A and 6B). The drug effect did not cause significant weight loss (fig. S3A).

After confirming the in vivo synergistic effect, we further tested whether the drug response was similar between the in vivo and in vitro models. First, a PDX-Organoids model was used to examine the drug reactivity (Fig. 6C) and the result showed that co-treatment with AZD5153 and Olaparib inhibited the spheroid growth, which was consistent with the findings in the PDX model. The immunohistochemistry results also showed changes in cell amplification and apoptosis that were similar to those observed in vitro (Fig. 6D). Then, we treated one of the PDX models with Olaparib for 3 months, during which we collected tumour samples for paraffin sectioning (Fig. 6E). The FISH assay was used to amplify the *PTEN* gene over time and the results were consistent with those obtained in vitro.

C57bl/6 mice were intraperitoneally implanted with the ID8 ovarian cancer cell line and after 21 days of drug treatment, the tumour was measured using the in vivo small animal imaging technology (SIEMENS Inveon). The results showed a lower tumour burden in the co-treated group (Fig. 6F). This abdominal tumour model compensated for the deficiency in the nude mouse model, which was immune-deficient. Both in vivo models produced the same result, which verified the synergistic effect of AZD5153 and Olaparib in vitro.

4. Discussion

In this study, we demonstrated the synergistic effect of AZD5153 and Olaparib in multiple models and successfully used PDO models in experiments that are usually based on cell lines. The results indicated that the PDO models could be used to confirm the combined effect of AZD5153 and Olaparib and further elucidate the mechanism of their synergistic action in ovarian cancer. The consistent results obtained in these models suggest the wide applicability of PDO and PDX model, which would allow exploration of the mechanisms of drug actions to be personalized. For patients with refractory ovarian cancer who do not benefit from most clinically used drugs, the discovery of personalized drug-resistant mechanisms may facilitate the development of curative treatments.

The increase in DNA replication stress was confirmed to be affected by BRD4 and PARP inhibitors in a previous study[11]. This difference in signalling pattern, where Olaparib induce more new DNA fibre suggests that this agent triggered the increase of DNA replication stress [31], which stimulated the replication of more DNA fibres. These results confirm that the marked synergistic cytotoxicity was mediated by the instability induced in DNA fibres. The presence of micronuclei reflects damage to hereditary cellular material and the increase induced by co-treatment with both agents was indicative widespread chromosomal breakage.

Our results indicated that phosphatase and tensin homolog (PTEN) was essential in the development of Olaparib resistance. After Olaparib treatment, ovarian cancer cells attempt to evade the lethal effect by enhancing the stability of genetic material including DNA and chromosomes by upregulating PTEN. This process can be prevented using AZD5153. Increased expression levels of PTEN were associated with a lower CI value, which reflects the strength of the effect of co-treatment with both agents on PTEN expression. Consequently, these findings also suggested a stronger response to co-treatment with AZD5153 and Olaparib and that their synergistic effect was mediated by their combined effects on PTEN expression.

In addition, we encountered some unexplained challenges in the exploration of the mechanism underlying the synergistic effect of both agents. PTEN is well known to negatively regulate phosphoinositide 3-kinase (PI3K) and the downstream AKT protein. However, as an inhibitor of BRD4, AZD5153 also strongly bind to enhancers [32, 33] of various genes and decreases their expression, which could counter the antagonistic effect of PTEN and PI3K. A previous study suggested that co-treatment with PARP and PI3K inhibitors exerts a stronger inhibitory effect on PTEN-deficient cancer [34]. In our study, AZD5153 reduced PTEN and PI3K simultaneously, which mimics the effect of PTEN deficiency and PI3K inhibition. We considered PTEN and not PI3K to be the key molecule because it is more strongly associated with the stability of hereditary material. Furthermore, the change in downstream RAD51 was consistent with that in PTEN [35]. However, the downstream mechanisms mediating the role of PTEN still need further investigation.

This study had some limitations, which are worth mentioning. Organoid cultures are easier to establish using more malignant tumours [36], mainly because of they have a lower level of differentiation and higher stemness than less malignant tumours. During model establishment, we obtained a higher success rate with high-grade serous ovarian cancer than we did with other less virulent samples, which may have caused selection bias. To avoid the influence of this selection bias, we used multiple models to confirm our conclusions. During the experiment, we also found that even with the same patient, differences occurred in drug responses. The drug responsiveness led us to infer that tumour cells isolated from ascites had the highest activity and drug resistance, and this was likely because they had an innate ability to survive as spheroids. [37]. However, the reason for the higher drug resistance of tumour cells in ascites has not been fully elucidated yet.

In conclusion, we present strong evidence supporting the notion that AZD5153 and Olaparib have a widespread synergistic effect. Olaparib treatment upregulates PTEN, leading to increased DNA and chromosome stability will rise, with accompanied acquired resistance cells. AZD5153 sensitizes cells to Olaparib and reverse the acquired resistance by down-regulating PTEN expression levels to destabilize hereditary materials. In this study, we used the following multiple ovarian cancer models PDX, PDO, and 3D/2D cell-lines to elucidate the co-effect of AZD5153 and Olaparib in vivo and in vitro. The similar results of these models further proved that the mechanism identified was consistent with the biological process occurring in ovarian cancer patients after drug treatment. This, consistency between results of different models suggest the possibility of translating these laboratory research findings into clinical studies towards developing treatments.

Declarations

1. Ethics approval and consent to participate

Animal experiments in this study were approved by the Institutional Animal Care and Use Committee at Tongji Medical Collage of Huazhong University of Science and Technology and the ethics number was TJH-201906004. The studies involving human participants were reviewed and approved by Tongji Medical College, Huazhong University of Science and Technology.

2. Consent for publication

All authors(Yuhan Huang, Chen Liu, Lixin You, Xi Li, Chaoyang Sun) have agreed “Synergistic effect of PARP inhibitor and BRD4 inhibitor in multiple models of ovarian cancer” to be published in ***cell and bioscience***.

3. Availability of data and materials

Data sharing not applicable to this article as no datasets were generated or analysed during the current study.

4. Competing interests

We confirm that this work is original and has not been published elsewhere, nor is it currently under consideration for publication elsewhere. We declare that there are no competing interests.

5. Funding

This work was supported by a National Natural Science Foundation (2020BCA067) and the Fundamental Research Funds for the Central Universities, Hust:2020JYCXJJ016 and 2020JYCXJJ014.

6. Author contributions

Gang Chen: Conceptualization and Funding acquisition.

Yuhan Huang: Investigation, Project administration, and Methodology.

Yuhan Huang: original draft.

Chen Liu: Data curation, Software, and Formal analysis.

Lixin You, Xi Li, Chaoyang Sun: Supervision and Validation.

7. Acknowledgments

Thanks to Chen Gang for providing ideas and financial support, thanks to Huili Hu for providing technical guidance, and thanks to everyone in the research team for their help.

References

1. Siegel R, Miller K, Jemal A. Cancer statistics, 2019. *CA: a cancer journal for clinicians* 2019, **69**(1): 7-34.
2. Lheureux S, Braunstein M, Oza A. Epithelial ovarian cancer: Evolution of management in the era of precision medicine. *CA: a cancer journal for clinicians* 2019, **69**(4): 280–304.
3. Christie E, Bowtell D. Acquired chemotherapy resistance in ovarian cancer. *Annals of oncology: official journal of the European Society for Medical Oncology* 2017, **28**: viii13-viii15.

4. Chiappa M, Guffanti F, Bertoni F, Colombo I, Damia G. Overcoming PARPi resistance: Preclinical and clinical evidence in ovarian cancer. *Drug resistance updates: reviews and commentaries in antimicrobial and anticancer chemotherapy* 2021: 100744.
5. González-Martín A, Pothuri B, Vergote I, DePont Christensen R, Graybill W, Mirza M, *et al.* Niraparib in Patients with Newly Diagnosed Advanced Ovarian Cancer. *The New England journal of medicine* 2019, **381**(25): 2391–2402.
6. Andrikopoulou A, Liontos M, Koutsoukos K, Dimopoulos M, Zagouri F. Clinical perspectives of BET inhibition in ovarian cancer. *Cellular oncology (Dordrecht)* 2021.
7. Karakashev S, Zhu H, Yokoyama Y, Zhao B, Fatkhutdinov N, Kossenkov A, *et al.* BET Bromodomain Inhibition Synergizes with PARP Inhibitor in Epithelial Ovarian Cancer. *Cell reports* 2017, **21**(12): 3398–3405.
8. Zhang P, Li R, Xiao H, Liu W, Zeng X, Xie G, *et al.* BRD4 Inhibitor AZD5153 Suppresses the Proliferation of Colorectal Cancer Cells and Sensitizes the Anticancer Effect of PARP Inhibitor. *International journal of biological sciences* 2019, **15**(9): 1942–1954.
9. Miller A, Fehling S, Garcia P, Gamblin T, Council L, van Waardenburg R, *et al.* The BET inhibitor JQ1 attenuates double-strand break repair and sensitizes models of pancreatic ductal adenocarcinoma to PARP inhibitors. *EBioMedicine* 2019, **44**: 419–430.
10. Wilson A, Stubbs M, Liu P, Ruggeri B, Khabele D. The BET inhibitor INCB054329 reduces homologous recombination efficiency and augments PARP inhibitor activity in ovarian cancer. *Gynecologic oncology* 2018, **149**(3): 575–584.
11. Sun C, Yin J, Fang Y, Chen J, Jeong K, Chen X, *et al.* BRD4 Inhibition Is Synthetic Lethal with PARP Inhibitors through the Induction of Homologous Recombination Deficiency. *Cancer cell* 2018, **33**(3): 401-416.e408.
12. Liu C, Zha Z, Zhou C, Chen Y, Xia W, Wang YN, *et al.* Ribonuclease 7-driven activation of ROS1 is a potential therapeutic target in hepatocellular carcinoma. *J Hepatol* 2020.
13. Vlachogiannis G, Hedayat S, Vatsiou A, Jamin Y, Fernández-Mateos J, Khan K, *et al.* Patient-derived organoids model treatment response of metastatic gastrointestinal cancers. *Science (New York, NY)* 2018, **359**(6378): 920–926.
14. Maru Y, Tanaka N, Itami M, Hippo Y. Efficient use of patient-derived organoids as a preclinical model for gynecologic tumors. *Gynecologic oncology* 2019, **154**(1): 189–198.
15. Rivera M, Fichtner I, Wulf-Goldenberg A, Sers C, Merk J, Patone G, *et al.* Patient-derived xenograft (PDX) models of colorectal carcinoma (CRC) as a platform for chemosensitivity and biomarker analysis in personalized medicine. *Neoplasia (New York, NY)* 2021, **23**(1): 21–35.
16. Yoshida G. Applications of patient-derived tumor xenograft models and tumor organoids. *Journal of hematology & oncology* 2020, **13**(1): 4.
17. Xu R, Zhou X, Wang S, Trinkle C. Tumor organoid models in precision medicine and investigating cancer-stromal interactions. *Pharmacology & therapeutics* 2021, **218**: 107668.

18. Byrne A, Alférez D, Amant F, Annibali D, Arribas J, Biankin A, *et al.* Interrogating open issues in cancer precision medicine with patient-derived xenografts. *Nature reviews Cancer* 2017, **17**(4): 254–268.
19. Beshiri M, Tice C, Tran C, Nguyen H, Sowalsky A, Agarwal S, *et al.* A PDX/Organoid Biobank of Advanced Prostate Cancers Captures Genomic and Phenotypic Heterogeneity for Disease Modeling and Therapeutic Screening. *Clinical cancer research: an official journal of the American Association for Cancer Research* 2018, **24**(17): 4332–4345.
20. Ledermann J, Harter P, Gourley C, Friedlander M, Vergote I, Rustin G, *et al.* Olaparib maintenance therapy in platinum-sensitive relapsed ovarian cancer. *The New England journal of medicine* 2012, **366**(15): 1382–1392.
21. Leo E, Johannes J, Illuzzi G, Zhang A, Hemsley P, Bista MJ, *et al.* Abstract LB-273: A head-to-head comparison of the properties of five clinical PARP inhibitors identifies new insights that can explain both the observed clinical efficacy and safety profiles. *Cancer Research* 2018, **78**(13 Supplement): LB-273-LB-273.
22. Murai J, Huang S, Renaud A, Zhang Y, Ji J, Takeda S, *et al.* Stereospecific PARP trapping by BMN 673 and comparison with olaparib and rucaparib. *Molecular cancer therapeutics* 2014, **13**(2): 433–443.
23. Murai J, Huang S, Das B, Renaud A, Zhang Y, Doroshow J, *et al.* Trapping of PARP1 and PARP2 by Clinical PARP Inhibitors. *Cancer research* 2012, **72**(21): 5588–5599.
24. Xu K, Chen D, Qian D, Zhang S, Zhang Y, Guo S, *et al.* AZD5153, a novel BRD4 inhibitor, suppresses human thyroid carcinoma cell growth in vitro and in vivo. *Biochemical and biophysical research communications* 2018, **499**(3): 531–537.
25. Zhang J, Dulak A, Hattersley M, Willis B, Nikkilä J, Wang A, *et al.* BRD4 facilitates replication stress-induced DNA damage response. *Oncogene* 2018, **37**(28): 3763–3777.
26. Quinet A, Carvajal-Maldonado D, Lemacon D, Vindigni A. DNA Fiber Analysis: Mind the Gap! *Methods in enzymology* 2017, **591**: 55–82.
27. Quinet A, Tirman S, Jackson J, Šviković S, Lemaçon D, Carvajal-Maldonado D, *et al.* PRIMPOL-Mediated Adaptive Response Suppresses Replication Fork Reversal in BRCA-Deficient Cells. *Molecular cell* 2020, **77**(3): 461-474.e469.
28. Schlacher K, Christ N, Siaud N, Egashira A, Wu H, Jasin M. Double-strand break repair-independent role for BRCA2 in blocking stalled replication fork degradation by MRE11. *Cell* 2011, **145**(4): 529-542.
29. He J, Kang X, Yin Y, Chao K, Shen W. PTEN regulates DNA replication progression and stalled fork recovery. *Nature communications* 2015, **6**: 7620.
30. Colicchia V, Petroni M, Guarguaglini G, Sardina F, Sahún-Roncero M, Carbonari M, *et al.* PARP inhibitors enhance replication stress and cause mitotic catastrophe in MYCN-dependent neuroblastoma. *Oncogene* 2017, **36**(33): 4682–4691.
31. Maya-Mendoza A, Moudry P, Merchut-Maya J, Lee M, Strauss R, Bartek J. High speed of fork progression induces DNA replication stress and genomic instability. *Nature* 2018, **559**(7713): 279–284.

32. Yokoyama Y, Zhu H, Lee J, Kossenkov A, Wu S, Wickramasinghe J, *et al.* BET Inhibitors Suppress ALDH Activity by Targeting ALDH1A1 Super-Enhancer in Ovarian Cancer. *Cancer research* 2016, **76**(21): 6320–6330.
33. Shi J, Vakoc C. The mechanisms behind the therapeutic activity of BET bromodomain inhibition. *Molecular cell* 2014, **54**(5): 728–736.
34. Bian X, Gao J, Luo F, Rui C, Zheng T, Wang D, *et al.* PTEN deficiency sensitizes endometrioid endometrial cancer to compound PARP-PI3K inhibition but not PARP inhibition as monotherapy. *Oncogene* 2018, **37**(3): 341–351.
35. Zhao Q, Guan J, Zhang Z, Lv J, Wang Y, Liu L, *et al.* Inhibition of Rad51 sensitizes breast cancer cells with wild-type PTEN to olaparib. *Biomedecine & pharmacotherapie* 2017, **94**: 165–168.
36. Drost J, van Jaarsveld R, Ponsioen B, Zimberlin C, van Boxtel R, Buijs A, *et al.* Sequential cancer mutations in cultured human intestinal stem cells. *Nature* 2015, **521**(7550): 43–47.
37. Uruski P, Mikuła-Pietrasik J, Pakuła M, Budkiewicz S, Drzewiecki M, Gaiday A, *et al.* Malignant Ascites Promote Adhesion of Ovarian Cancer Cells to Peritoneal Mesothelium and Fibroblasts. *International journal of molecular sciences* 2021, **22**(8).

Figures

Figure 1. Olaparib treatment can enhance the expression of PTEN which relates to Olaparib resistance

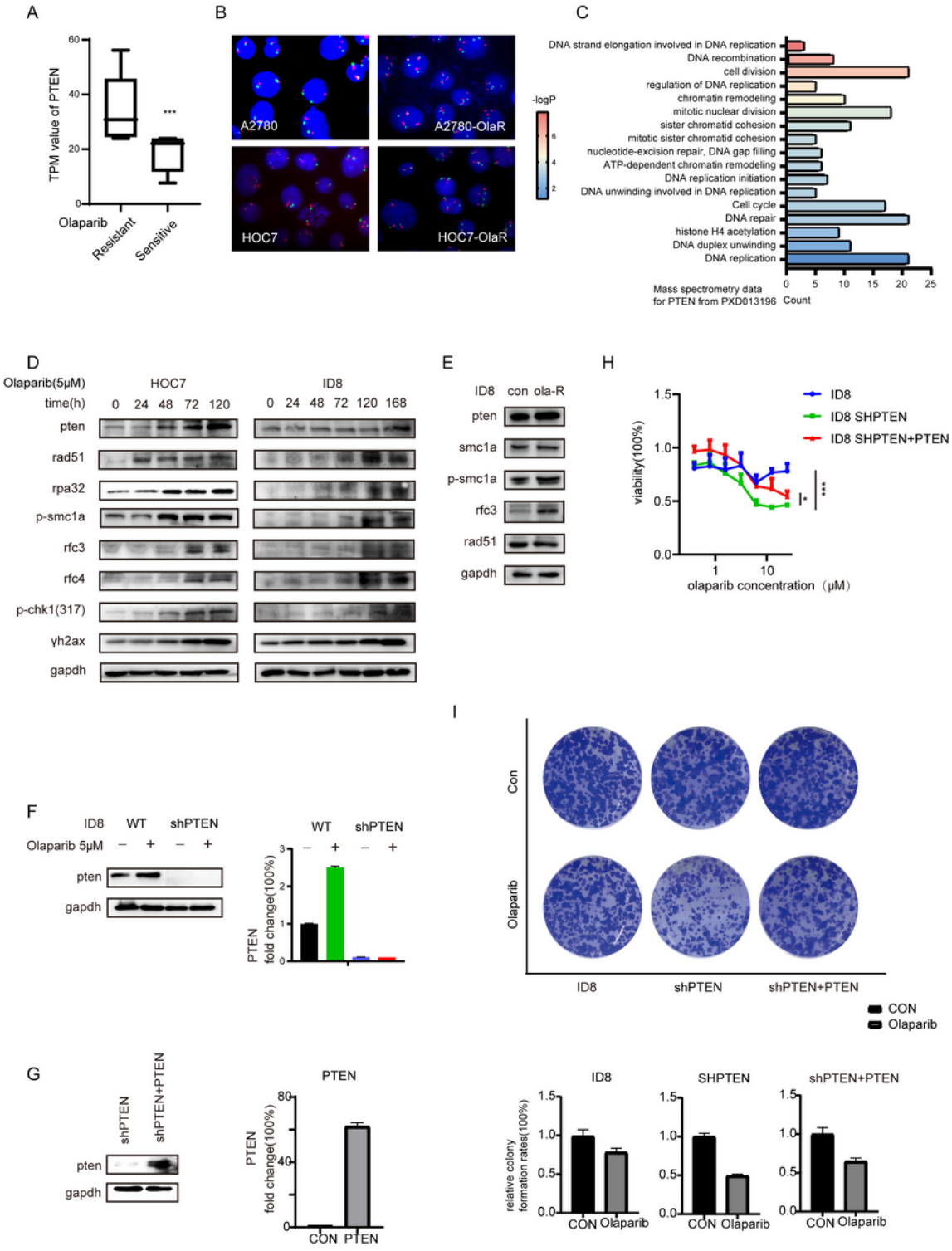

Figure 1

Olaparib treatment can enhance the expression of PTEN which relates to Olaparib resistance.

(A) From the RNA-seq data of PDO models tested before, relative resistant PDO models had higher PTEN expression than relative sensitive ones.

(B) FISH assay was used to detect the PTEN gene amplification of two Olaparib-resistant cell lines. After inducing drug resistance, the cells changed from the normal signal mode (two red and two green) to the PTEN gene amplification signal mode (mainly three red and three green).

(C) The mass spectrum data of PTEN suggested that PTEN has significant and close interaction with proteins in the above pathways. It includes various proteins related to chromosome stability and DNA replication forks.

(D) The change in protein expression showed by western blotting indicated that with Olaparib treatment, PTEN and the proteins related to DNA stability, chromosome stability, and replication pressure increased over time.

(E) Western blotting showed that the induced Olaparib resistant ID8-OlaR cells showed increased PTEN expression and chromosome, DNA stability related protein expression.

(F) The results of western-blotting and Q-RTPCR verified the downregulation of PTEN after shRNA treatment.

(G) The results of western-blotting and Q-RTPCR verified the upregulation of PTEN after overexpression virus treatment.

(H) The drug reactivity of ID8, ID8 shPTEN, and ID8 shPTEN+PTEN to Olaparib was shown. p-value from Student t-test: ns as nonsense, *P < 0.05, **P < 0.01, ***P < 0.001, ****P < 0.0001.

(I) Representative images of the clonogenic assay ID8, ID8 shPTEN, and ID8 shPTEN+PTEN in the presence of Olaparib for 10 days.

Figure 2. AZD5153 reverse Olaparib resistance by reducing PTEN expression

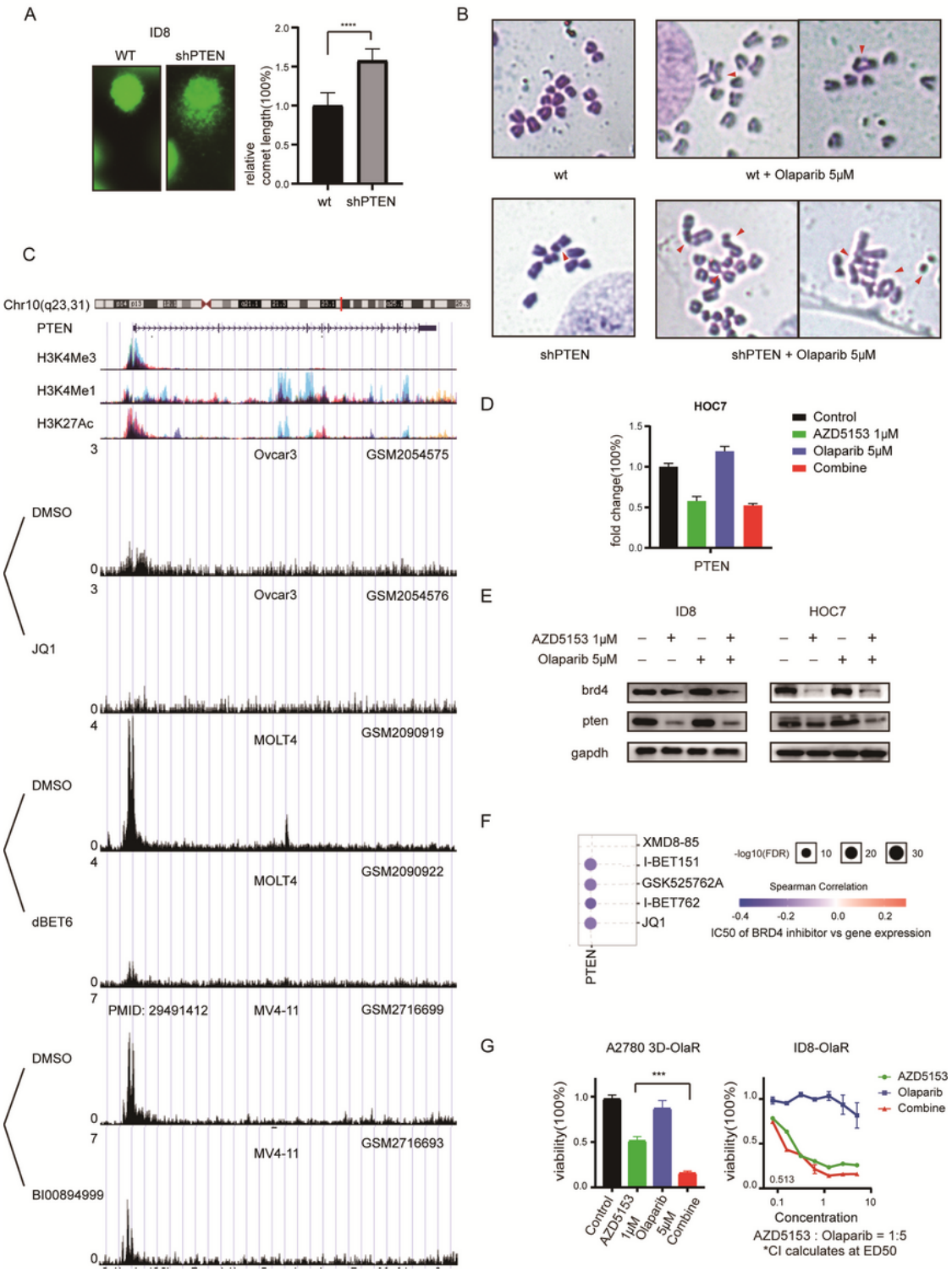

Figure 2

AZD5153 reverse Olaparib resistance by reducing PTEN expression

(A) As shown in the comet assay, after shPTEN, endogenous DNA fragmentation increased, as DNA stability decreased.

(B) The chromosome of wild-type ID8 cells treated with Olaparib showed a DNA double-strand break repairing status, while shPTEN-ID8 cells had extensive complex aberrations, which indicates repairing disorder after damage.

(C) Chip-seq data from the public database was shown in this figure. BRD4 inhibitors can lower the expression of PTEN in different types of cancer, including ovarian cancer.

(D) The results of Q-RTPCR implied that AZD5153 can downregulate PTEN expression.

(E) The results of WB implied that AZD5153 can downregulate PTEN and BRD4 expression.

(F) According to CCLE, CTRP, and GDSC data, PTEN expression was negatively correlated with IC50 to various kinds of BRD4 inhibitors. To BRD4 inhibitors, higher expression of PTEN corresponding to higher sensitivity.

(G) The drug reactivity of 2D ID8-OlaR and 3D A2780-OlaR to AZD5153 was shown. The CI value of ID8 at ED50 was calculated, which indicated that the acquired resistant cells are still sensitive to combining treatment.

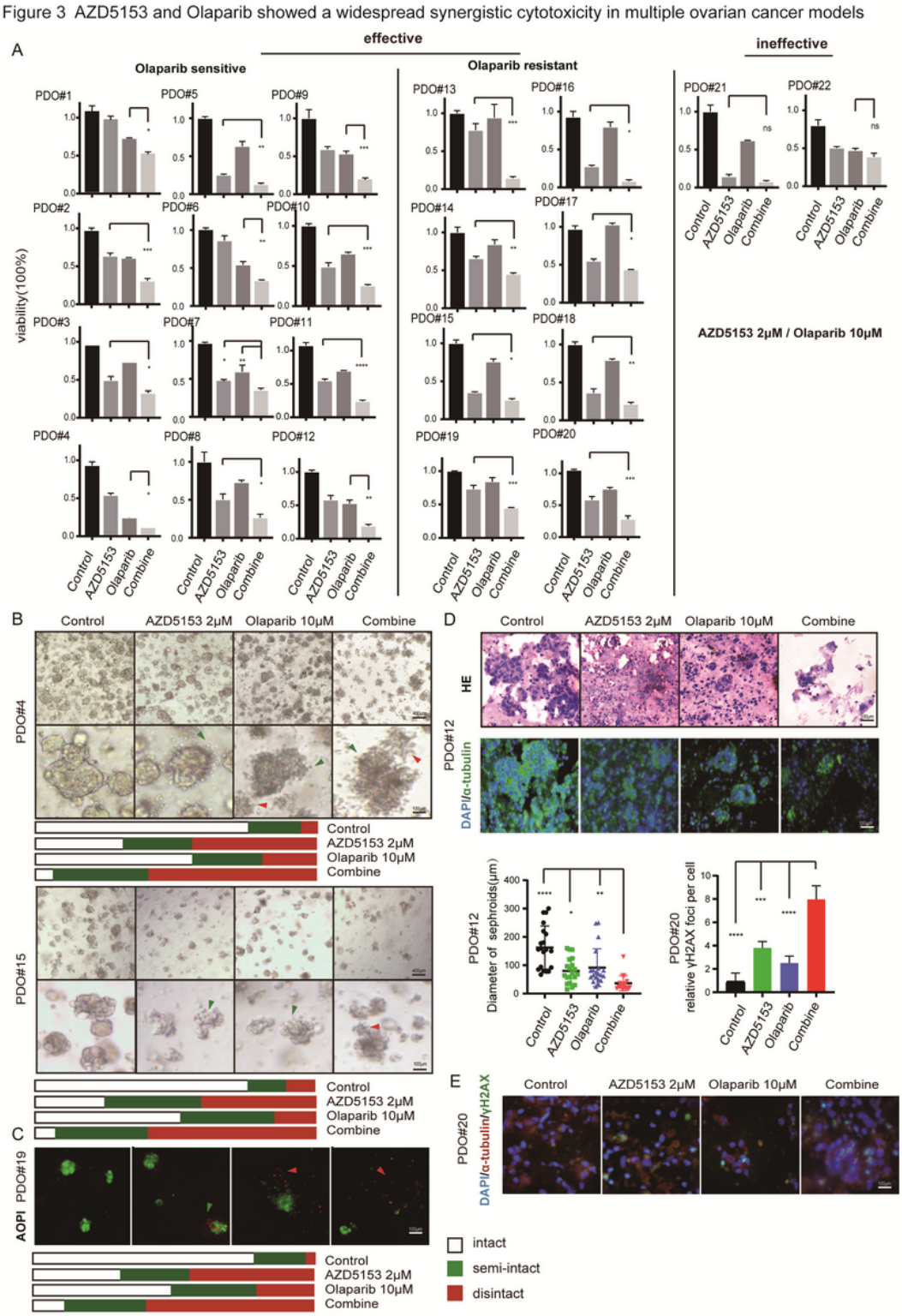

Figure 3

AZD5153 and Olaparib showed a widespread synergistic cytotoxicity in multiple ovarian cancer models

(A) The figure showed the drug reaction of 22 PDO models. The results were divided into groups according to the relative sensitivity to Olaparib. No matter how sensitive the tumor to a single drug alone, almost all the samples can benefit more after combining treatment.

(B) The figure showed the spheroid made of cell line under the 3D culture condition by bright field of microscope. The picture below is an enlargement of the one above. The spheroids are classified into different status, which were signed by arrows in the enlargement picture. The percentage was shown below.

(C) The figure showed the status of spheroids by AOPI staining, green light showed living cells, while the red light showed dead ones. The percentage of intact or semi-intact spheroids are shown below.

(D) The figure showed the size and density of PDO spheroids after slicing and staining. The diameter of spheroids was calculated, while the viability of PDO#12 in fig3A can show the entire status after drug treatment.

(E) The figure showed the change of γH2AX level after drug treatment.

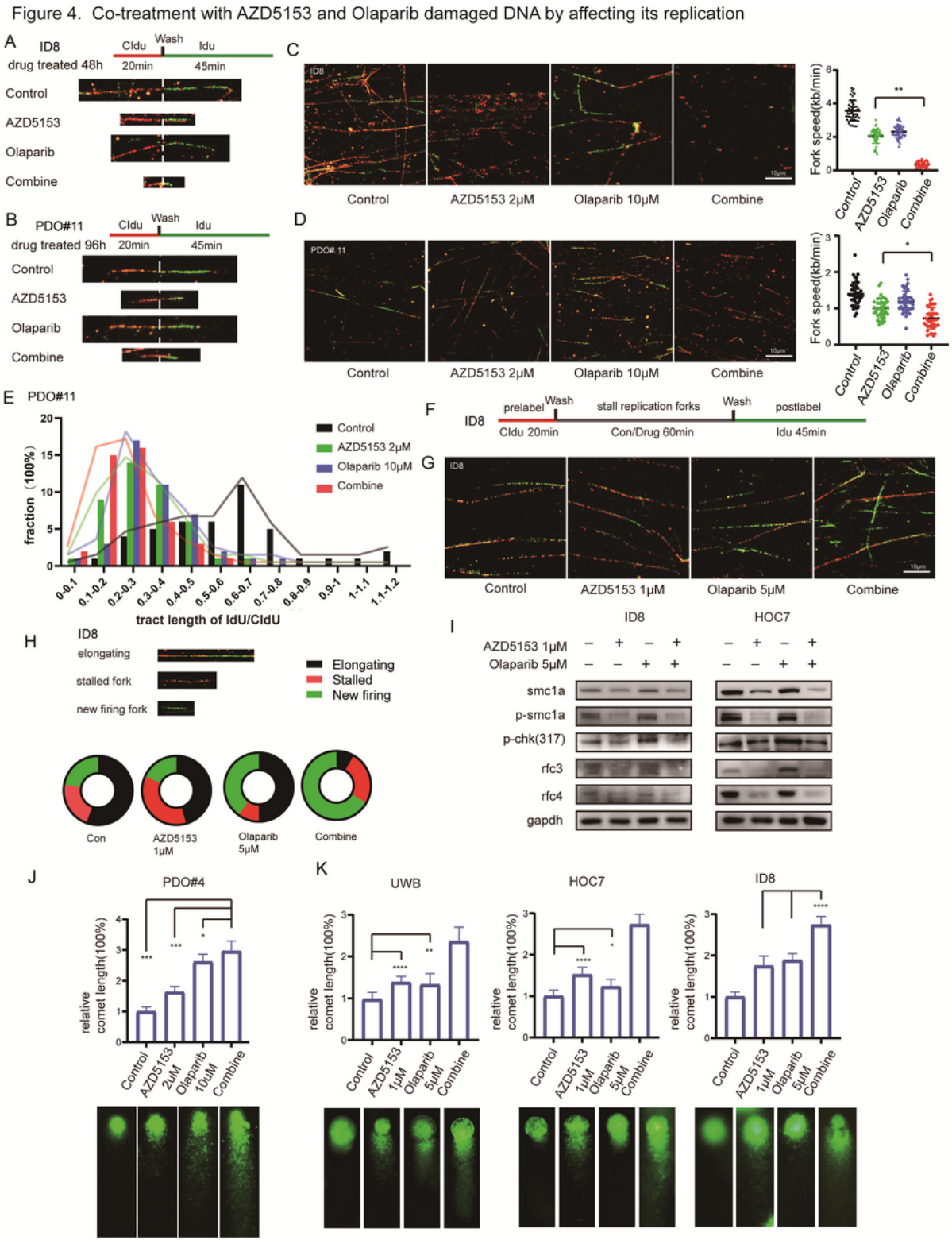

Figure 4

Co-treatment with AZD5153 and Olaparib damaged DNA by affecting its replication

(A) The figure showed the sequence of drug treating and fluorescence labeling of the ID8 cell line in DNA fiber assay. The drug was given before labeling.

(B) The figure showed the sequence of drug treating and fluorescence labeling of the PDO model. The typical status of DNA fibers in each group was also shown.

(C) In the figure, we can see the typical DNA fiber status of the ID8 cell line in each group and the statistical results of replication speed under the influence of drugs.

(D) In the figure, we can see the typical performance of PDO samples after drug treatment and the statistical results of replication speed in each group.

(E) The statistical results of the replication fork stability represented by the ratio of fluorescence length of CIdU to IdU in the ID8 cell line. The distribution range of the IdU / CIdU ratio was obtained by counting more than 50 DNA fibers.

(F) The sequence of drug treating and fluorescence labeling of ID8 was shown. The drug was given between labeling.

(G) The typical fluorescence type of each group in the DNA fiber test was shown in this figure. The combined group exhibited a typically short and dense green light.

(H) The graph showed the typical status of DNA fibers. The proportion of different types of DNA in different drug treatment groups was also shown.

(I) The picture showed the changes in proteins related to DNA replication fork stability and chromosome stability after the treatment of each group.

(J) The figure showed the results of the comet assay after 96 hours of drug treatment in the PDO model.

(K) Three cell lines with different single drug sensitivity to Olaparib or azd5153 were demonstrated. After 48 hours of drug treatment, the comet assay showed the strength of double-strand break in each group. The combined group showed a stronger double-strand break.

Figure 5. AZD5153 and Olaparib can also cause greater damage in chromosome and lead to apoptosis.

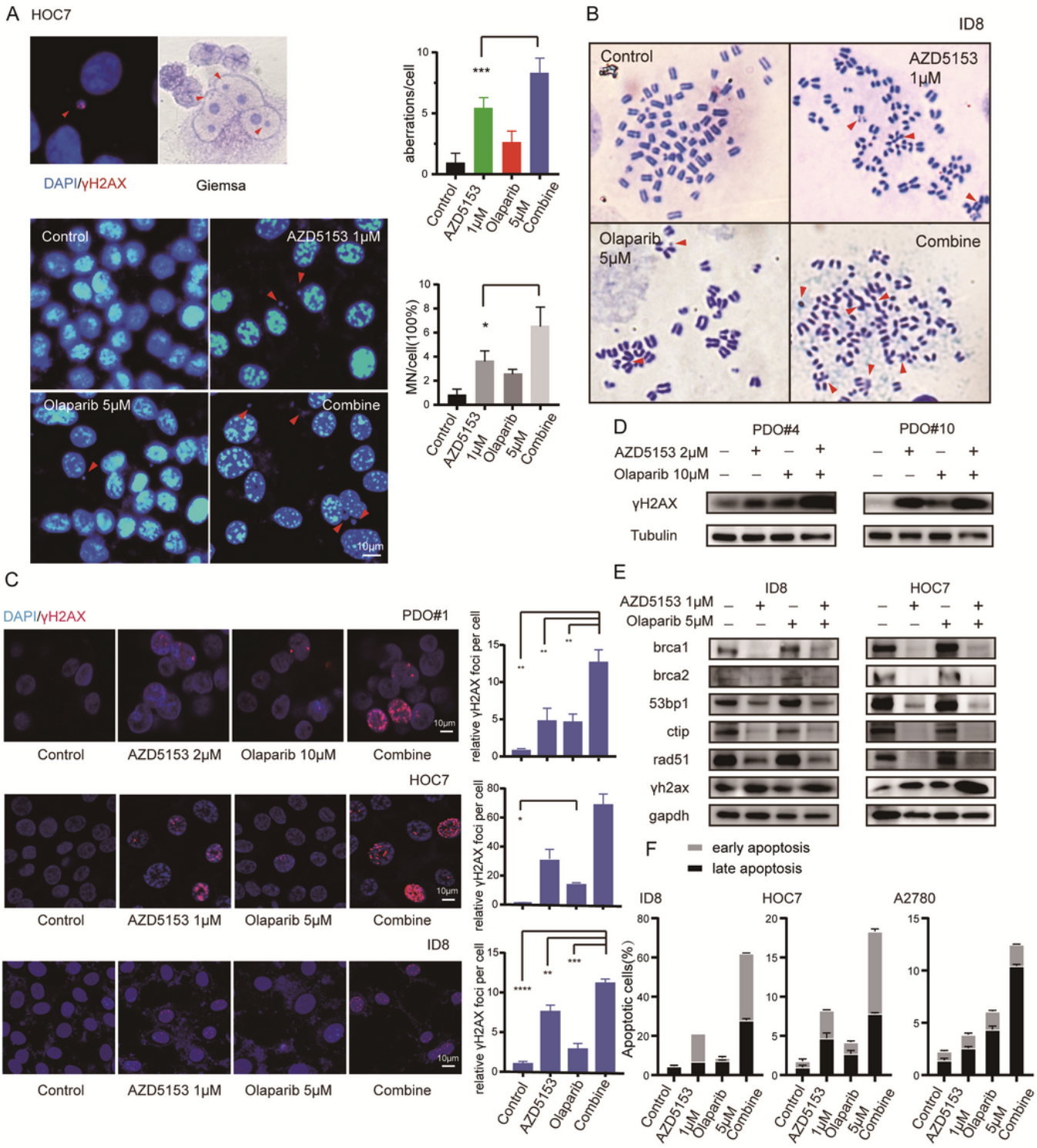

Figure 5

AZD5153 and Olaparib can also cause greater damage in chromosome and lead to apoptosis.

(A) The figure showed a typical micronucleus of the hoc7 cell line by DAPI/γH2AX staining and Giemsa staining. The percentage of micronucleus in each group after treatment was calculated by DAPI staining, which was also shown.

(B) The figure showed the results of the metaphase spread assay after the cell was treated with drugs. The arrow showed chromosome breakage and aberration. The percentage of chromosome breakage and aberration in each group after drug treatment was also shown.

(C) The figure showed the change of γH2AX expression in cell lines and the PDO model by immunofluorescent. The relative γH2AZ foci per cell were also shown.

(D) The figure showed the changes in protein expression of γH2AX.

(E) The changes in protein expression which relates to DNA damage and repair in cell lines was shown.

(F) The results of flow cytometry showed the percentage of apoptosis in cell lines after drug treatment.

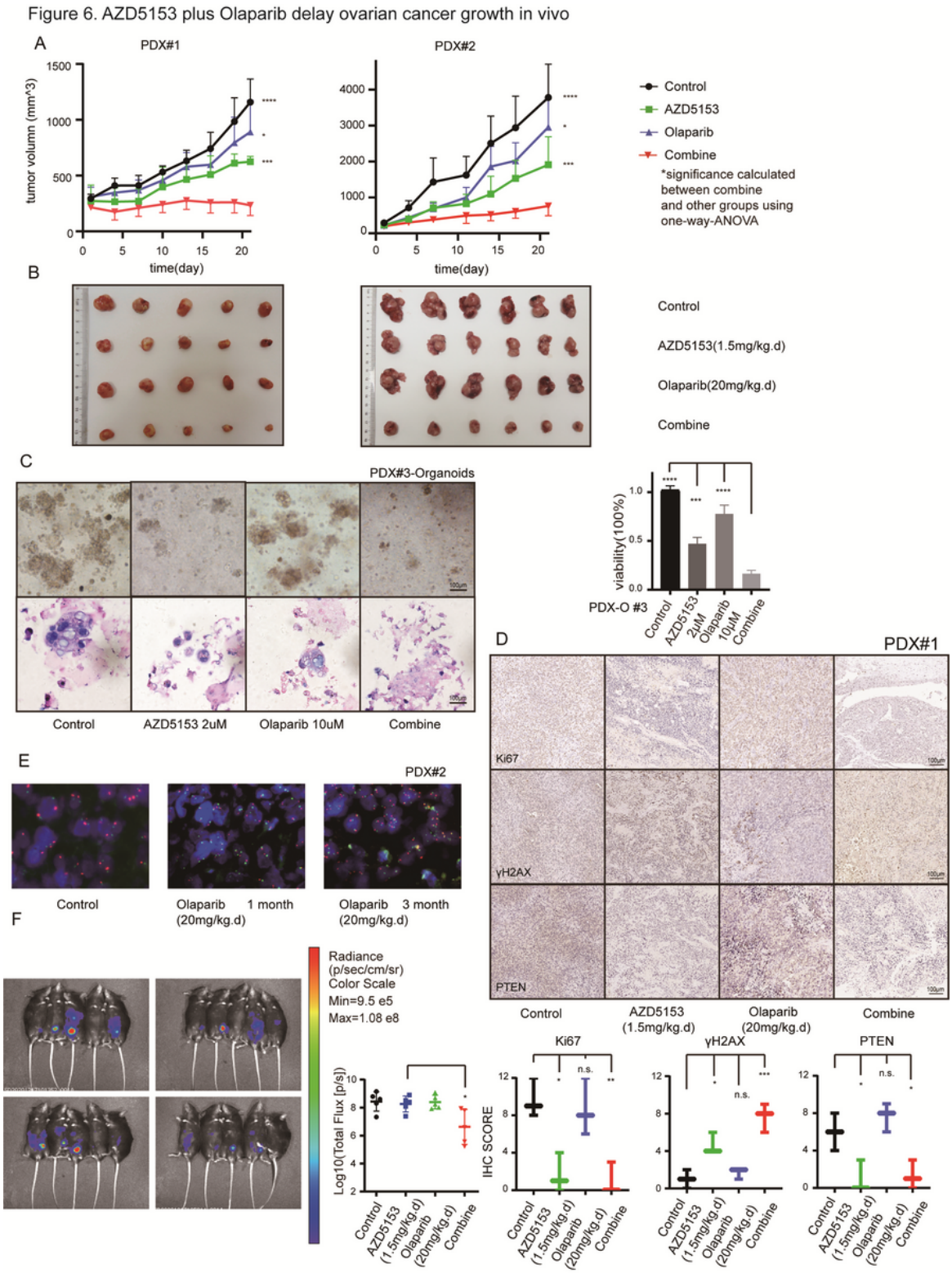

Figure 6

AZD5153 and Olaparib can delay ovarian cancer growth in vivo.

(A) Two cases of PDX models which were divided into four groups were given vehicle, AZD5153, Olaparib, and dual drugs respectively. The dosage was shown in the figure. The curve of tumor volume in 21 days is also shown.

(B)The figure showed the volume of tumor tissue which were taken after the mouse sacrificed after drug treatment for 21 days.

(C) After PDX-O culturing and drug treatment, the size, and density of the spheroids in each group were shown in a bright field of microscope and by HE staining. The entire status of viability was calculated by CELLTiter GLO 3D, which was shown in the right.

(D) Immunohistochemistry showed that the expression of Ki67, γH2AX, PTEN in PDX#2 tumor tissue was changed after treatment. The change was consistent with other results.

(E) The signal pattern of the FISH assay was performed before treatment, after one month, and after three months of Olaparib treatment. It was found that PTEN also amplificated along with Olaparib treatment in vivo.

(F) The figure showed the in vivo small animal imaging results of C57BL/6 mice planted by ID8 cells intraperitoneally and treated by drugs for 21 days. The combining group has lower average fluorescence intensity than other groups.

Supplementary Files

This is a list of supplementary files associated with this preprint. Click to download.

- Graphicabstract.tif
- supplement.doc